13th International Brick and
Block Masonry Conference
Amsterdam, July 4-7, 2004

DRIVING RAIN AND SOILING OF MASONRY FACADES

Blocken B.[1], Desadeleer W.[1] and J. Carmeliet[1*,2]

Abstract

A numerical method based on Computational Fluid Dynamics is applied for a preliminary study of the relationship between driving rain and building envelope pathology (facade surface disfigurement). The study is conducted for the case of the ceramic brick facade of a low-rise office building. It will be shown that the numerical method can be used to explain disfigurement patterns that are caused by direct driving rain impingement.

Key Words

Driving rain, Computational Fluid Dynamics, Soiling, Masonry

1 Introduction

Although building designers assume that building facades will retain their clean appearance, contemporary constructions are often an illustration of how climatic exposition can lead to disappointments by changes in surface appearance. Figure 1 illustrates disfigurement of a ceramic brick facade of a low-rise office building. Although the construction was only completed four years ago, surface soiling patterns have appeared at six different positions, indicated by 'p1' to 'p6'. Stains are present below the point where the terrace sill meets the free-standing wall (p1), along the free-standing building edge (p2), around the circular aperture at the left (p3), below the circular window at the right (p4) and at the top corners (p5 and p6). According to the company management, the surface soiling patterns have appeared shortly after building completion and have been persistent throughout the years.

Surface disfigurement of facades is often caused by the combined effect of atmospheric dirt deposition and driving rain impingement. Whereas atmospheric dirt deposition alone leads to an – often acceptable – evenly distributed soiling of the facade, the combination with driving rain is responsible for the occurrence of stains and streaks. In the case of Figure 1, patterns p1 and p4 are caused by rain water that is not retained or rejected by adequate detailing. The water is allowed to run off from the sill

[1] Laboratory of Building Physics, Department of Civil Engineering, Catholic University of Leuven, Kasteelpark Arenberg 51, 3001 Heverlee, Belgium
[2] Building Physics Group, Faculty of Building and Architecture, T.U.Eindhoven, P.O.Box 513, 5600 MB Eindhoven, The Netherlands
*Corresponding author: jan.carmeliet@bwk.kuleuven.ac.be

(p1) and the glass pane (p4). As a result, the dirt particles from these surfaces are washed away and redepositioned at the facade. Furthermore, Camuffo et al. (1982) note that wetted surfaces enormously enhance the collection efficiency of black airborne carbonaceous particles compared with the same surface in the dry state. Together with the knowledge that driving rain loads reach their highest values at the edges and top corners of a building, patterns p5 and p6, as well as p2 can be explained this way. The most significant pattern however is p3. This pattern is present around the circular aperture and is stretched towards the bottom left. No straightforward or easy explanation can be given for this pattern. Comparing the circular aperture at the left to the window with a similar geometry at the right, the aperture seems to be significantly increasing driving rain impingement. It is possible that the left facade with aperture acts as a flat plate concentrating wind and driving rain drops towards the circular aperture and depositing drops at the circumference. The explanation of the features of this pattern necessitates detailed knowledge of the behaviour of wind and rain near the building.

Until recently, information on driving rain on buildings was gathered by employing either an experimental or a semi-empirical approach. As research efforts continued to reveal the inherent complexity of the problem, researchers realised that further achievements were to be found through numerical analyses. In the past decade, Computational Fluid Dynamics (CFD) has made its introduction in the area. A number of researchers have employed CFD to study the trajectories of raindrops in the calculated wind flow pattern around a building and to determine the driving rain amount falling onto the building facade (Choi 1993, Wisse 1994, Sankaran & Paterson 1995, Lakehal et al. 1995, Karagiozis et al. 1997, van Mook et al. 1997, van Mook 1999, Hangan 1999, Etyemezian et al. 2000). Based on their investigations, a practical numerical simulation method for driving rain has been developed (Blocken & Carmeliet 2000a, 2000b). The method allows the calculation of both the spatial and temporal distribution of driving rain on buildings based on generally available climatic data (wind speed, wind direction, rainfall intensity). It has been verified and found to yield fairly accurate results for the case of a low-rise building and for different rain events (Blocken & Carmeliet 2000a, 2002).

In this paper, the numerical model is employed to examine and explain the observed staining pattern p3. A brief review of the numerical model will first be given in section 2. In section 3, the case study will be outlined, computed and analysed.

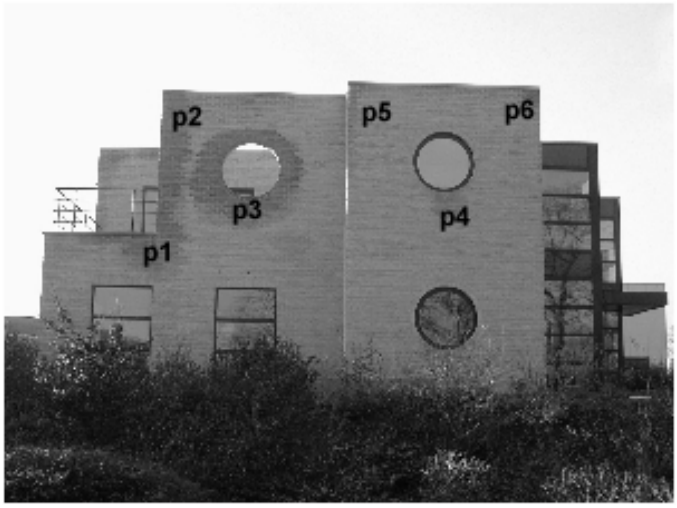

Figure 1. Surface soiling patterns at the ceramic brick facade of a low-rise office building.

2 Numerical model

The quantities that are used to describe the driving rain load are the specific catch ratio η_d (for one raindrop diameter d) and the catch ratio η (for all raindrop diameters) (Eq. 1):

$$\eta_d(t) = \frac{R_{dr}(d,t)}{R_h(d,t)} \quad , \quad \eta(t) = \frac{R_{dr}(t)}{R_h(t)} \tag{1}$$

where $R_{dr}(d,t)$ and $R_h(d,t)$ are the specific driving rain intensity and specific horizontal rainfall intensity (i.e. through a horizontal plane) for raindrops with diameter d (L/m²h or mm/h). $R_{dr}(t)$ and $R_h(t)$ refer to the same quantities but integrated over all raindrop diameters taking into account the raindrop spectrum. In the interest of brevity, only the headlines of the numerical model will be given here. To calculate the driving rain load on a building facade for a given climate data set, the following 6 steps of the numerical model must be executed (Blocken & Carmeliet 2000a, 2000b, 2002):

1. Calculation of the steady-state wind flow pattern around the building using a CFD (Computational Fluid Dynamics) code. The Reynolds Averaged Navier-Stokes equations and the continuity equation are solved. Closure is obtained by employing a version of the k-ε turbulence model.
2. Calculation of raindrop trajectories in the flow pattern by solving their equation of motion.
3. Determination of the specific catch ratio (i.e. the ratio of driving rain to horizontal rainfall) from the configuration of the raindrop trajectories. The calculation of the specific catch ratio is performed for a number of zones on the building facade with a surface A_f. In a steady-state wind flow pattern - thus neglecting turbulent dispersion of raindrops - raindrop trajectories of diameter d ending on the corner points of the zone form a stream tube. Conservation of mass for the raindrops allows η_d to be expressed in terms of areas: (Eq. 2):

   $$\eta_d(d) = \frac{R_{dr}(d)}{R_h(d)} = \frac{A_h(d)}{A_f} \tag{2}$$

   where A_f is the area of the zone on the building facade where η_d is to be determined, and $A_h(d)$ is the area of the horizontal plane bounded by the injection positions of the raindrops of diameter d ending on the corner points of A_f. This plane A_h is located in the upstream undisturbed wind flow. Its location must allow the raindrops injected at that position to reach their terminal velocity of fall (vertical) and the wind velocity (horizontal) before entering the flow pattern disturbed by the presence of the building and its surroundings.
4. Calculation of the catch ratio based on the specific catch ratio and the raindrop spectrum.
5. Transformation of the climatic data set into a “representative climate data set for driving rain estimation” using a specific weighted averaging technique (Blocken & Carmeliet 2000b).
6. Calculation of the driving rain load at each facade position as a function of time by combining the results from step 4 and 5.

Step 1 to 4 correspond to the steady-state simulation technique that was first developed by Choi (1993) and has been employed by a large number of researchers since then. This procedure yields the driving rain amount at a certain building envelope position under steady-state conditions of wind and rain. Steps 5 and 6 extend the

method into the time domain. Experimental verification of steps 1 to 4 has been made by van Mook (1999) and Hangan (1999). Experimental verification of the complete numerical procedure (steps 1 to 6) has been performed by Blocken & Carmeliet (2000a, 2000b, 2002). More information can be found in these references.

3 Numerical study of driving rain

3.1 Problem statement

The building under study is an industrial building, comprising an office building integrated in a factory building. It is situated in Herent, a village near Leuven. Figure 1 illustrates the east facade of the building.

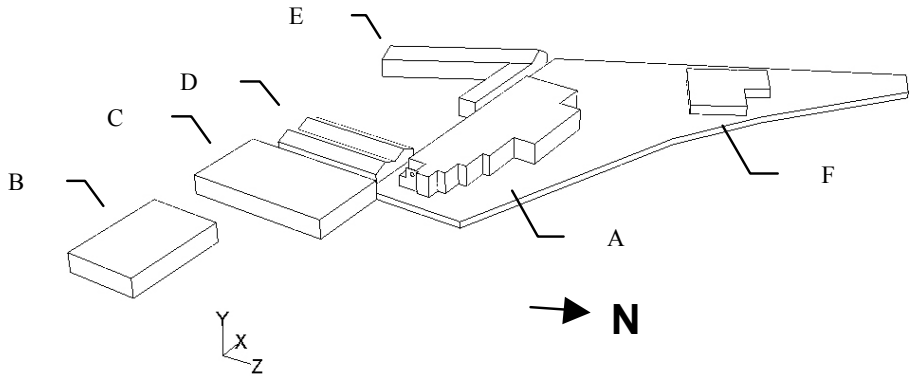

Figure 2. Perspective view of the site with the industrial building (A) and the surrounding buildings (B-F)

Figure 2 yields a perspective view of the site with the industrial building (A) and the surrounding buildings. The surrounding buildings are indicated as buildings B – F. Buildings A and F are located on a plateau rising 2 m above local ground level, causing building A to be the highest building. Maximum length, width and height of building A are 66.0 m, 25.0 m and 6.6 m respectively. The total width of the east brick facade shown in Figure 1 is 10.6 m. The left part of this facade has a backward recession of 0.8 m compared to the right part. At the first floor in the south-east building corner, a terrace was constructed, with a free-standing wall that exhibits a 0.65 m radius circular aperture. The building was constructed with a light coloured ceramic brick showing a high water absorption coefficient (A = 0.36 kg/m²s$^{1/2}$) and a capillary moisture content of about 260 kg/m³.

3.2 Numerical modelling

To understand the phenomena leading to pattern p3, numerical modelling is employed. It is noted that the model, in its present state, only addresses “direct” driving rain impact and does not account for run-off across the surface and for moisture transport in porous media. However, given the properties of the brick (see section 3.1), runoff starting from the brick surface itself is not very likely and we should be able to explain pattern p3 by the present model.
In this paper, we limit ourselves to steps 1 to 3 of the numerical model (section 2) and we will calculate wetting for a number of weather conditions. Three wind directions are

selected for the analysis: east (108°, figure 1), south-west (225°) and west (288°). Apart from selecting the wind direction perpendicular to the facade under study (east), wind directions west and south-west were also chosen for two reasons: (1) the prevalence of these directions in wind statistics and (2) the site geometry.
Wind from these directions is less obstructed by buildings B, C, D and E and will be channelled through the passage between buildings A and C-D. The model of the buildings is placed in a computational domain that is discretised by means of about $2*10^6$ tetrahedral control volumes. Part of the surface mesh on the buildings is shown in Figure 3. At the inlet of the computational domain, a logarithmic wind profile is specified. Roughness length z_0 is taken 0.25 m according to the updated Davenport roughness classification (Wieringa 1992). Local ground and building surface roughness $z_{0,loc}$ and $z_{0,b}$ are taken 0.01 m. Symmetry conditions are imposed at the upper and side boundaries. The simulations are performed on an unstructured, tetrahedral grid using a commercial CFD code (Fluent). The realizable k-ε model developed by Shih et al. (1995) was used in combination with two-layer based non equilibrium wall functions (Kim & Choudhury 1995) as they have been shown to perform better than their standard counterparts and to be more suitable for complex flows involving strong adverse pressure gradients, separation and recirculation (Kim & Choudhury 1995, Kim et al. 1997).

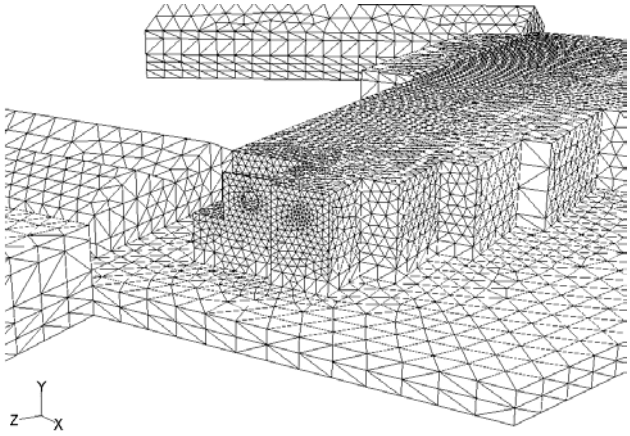

Figure 3. Numerical grid configuration at the building surfaces.

The steady-state wind flow pattern is calculated for nine combinations of wind direction (108°, 225°, 288°) and reference wind speed (U_{10} = 1 m/s, 5 m/s, 8 m/s). The reference wind speed is the upstream unobstructed wind speed at 10 m height. Results are given in Figure 4 for each wind direction. Wind velocity contours are indicated in a horizontal plane cutting at mid-height through the circular aperture. Wind velocity vectors are displayed in a horizontal plane and in a vertical plane, respectively at mid-height and midway through the circular aperture. The oversized arrow indicates the upstream unobstructed wind direction. Following observations are made (Fig. 4):
ϕ = 108°. The wind flows fairly unobstructed towards the east facade of the office building. The wind is deflected at the vertical building edges, at the terrace horizontal edge, at the top of the facade and through the circular aperture causing increased wind speed at these positions. At the terrace, behind the free-standing wall, a recirculation zone develops.
ϕ = 225°. The wind flow is guided by the surrounding buildings. Wind is forced to flow between buildings D and E and subsequently between buildings D-C and A, causing increased wind speed in these passages. High wind velocities are observed especially near the vertical edge of the free-standing wall and above the roof of building A and the

top edge of the free-standing wall. Wind speed in the circular aperture is limited. Except from the south-east corner, most of the terrace is shielded from wind.

ϕ = 288°. The oncoming wind is deflected around and over building A. A skimming flow along and over the terrace is observed in the horizontal and the vertical plane respectively. As a result, wind velocity is high near the top edge of the free-standing wall. Near the vertical edge of this wall, wind speed is limited, as this edge is recessed compared to the long south building wall. Wind flow through the circular aperture is negligible. The terrace is completely shielded from wind.

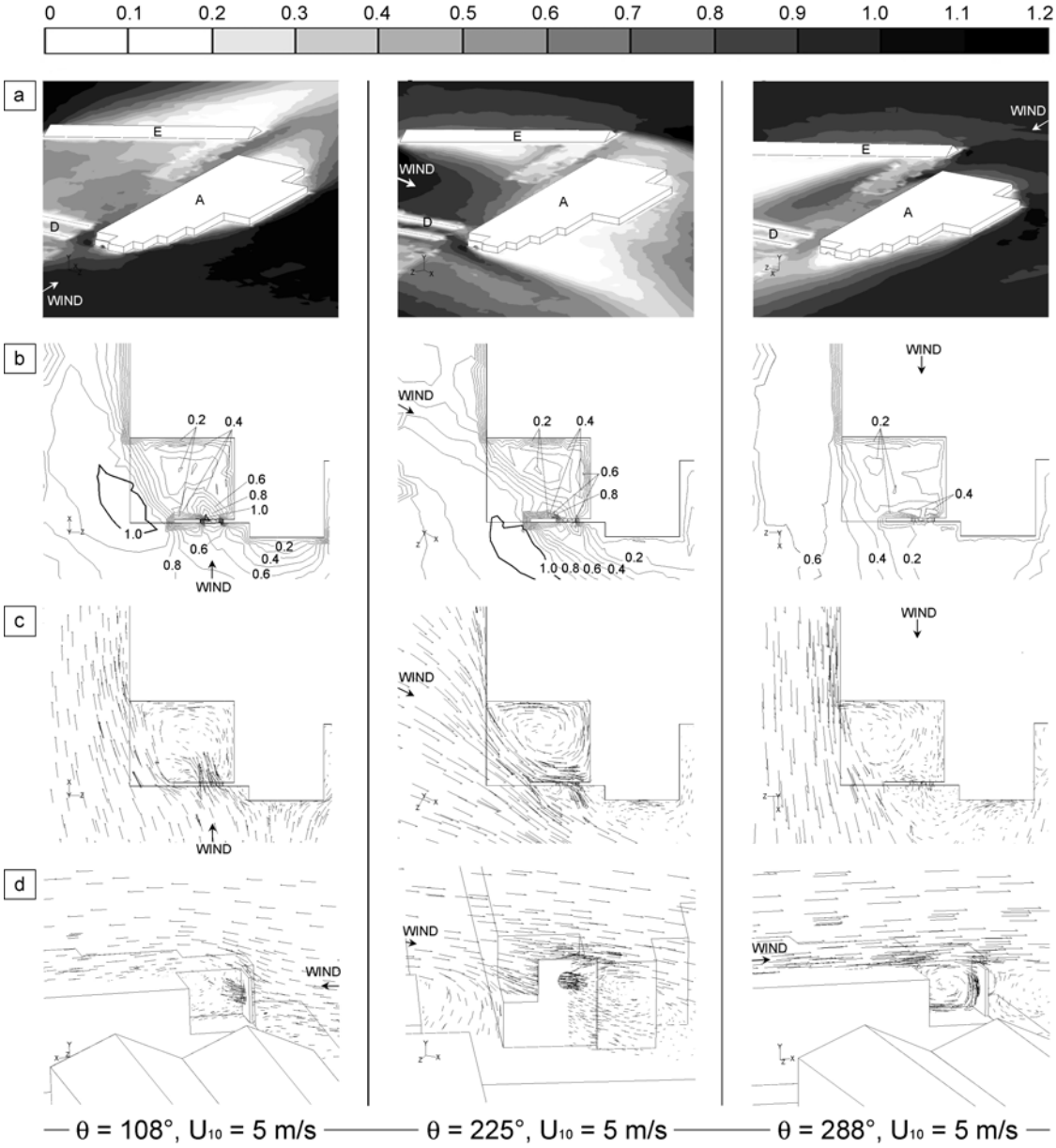

Figure 4. (a) Contours of dimensionless wind velocity (local wind speed divided by reference wind speed, i.e. the undisturbed upstream wind speed at 10 m height). The contours are displayed in a horizontal plane through the centre of the circular aperture for θ = 108°, θ = 225°, θ = 288°. (b) Local contours of dimensionless wind speed in the same horizontal plane. (c) Wind velocity vectors in the same horizontal plane. (d) Wind velocity vectors in a vertical plane through the centre of the circular aperture.

For each of the wind flow patterns calculated, 3D Lagrangian particle tracking is performed for raindrops of small (0.5 mm), moderate (1 mm) and large (5 mm) size. From the configuration of the raindrop trajectories, the specific catch ratio is calculated. It is a measure for the amount of driving rain falling onto different parts of the facade. Results for the three wind directions are given in Figure 5 to 7. Contours of the specific catch ratio are displayed at the wetted face (east facade for ϕ = 108°, west face of free-standing wall for ϕ = 225° and 288°). Results are given for 1 mm raindrops. Results for 0.5 mm and 5 mm drops indicate the same phenomena. Distinct wetting patterns are observed:

ϕ = 108°. (Fig. 5). The specific catch ratio increases from bottom to top of the facade. High values are found where wind speed is large: at the top edge, at the vertical edges (descending contour lines), at the left corner below the terrace sill and round the circular aperture. It is noted that neither the sill nor the 3 cm roof overhang at the top edge were included in the model. From an earlier study (see Blocken and Carmeliet 2002), it has become clear that such small details can provide significant shelter in their immediate vicinity, but that their effect on overall rain distribution is small. The specific catch ratio at these positions is thus overestimated in the simulation.

Let us focus on the circular aperture and compare observations to the circular window at the right. Increased wetting is observed near the circular aperture as contour lines show a sudden drop. For U_{10} = 5 m/s and 8 m/s, the wetting pattern is clearly stretched towards the left (cfr. Fig. 1). This is because the wind passing through the aperture is forced to flow to the left because of the configuration of the terrace behind. The raindrops follow the wind flow. Specific catch ratio values at this position are on average about 40% of those near the window at the right. Remark: the recession of the left part of the facade introduces contour irregularities at this position.

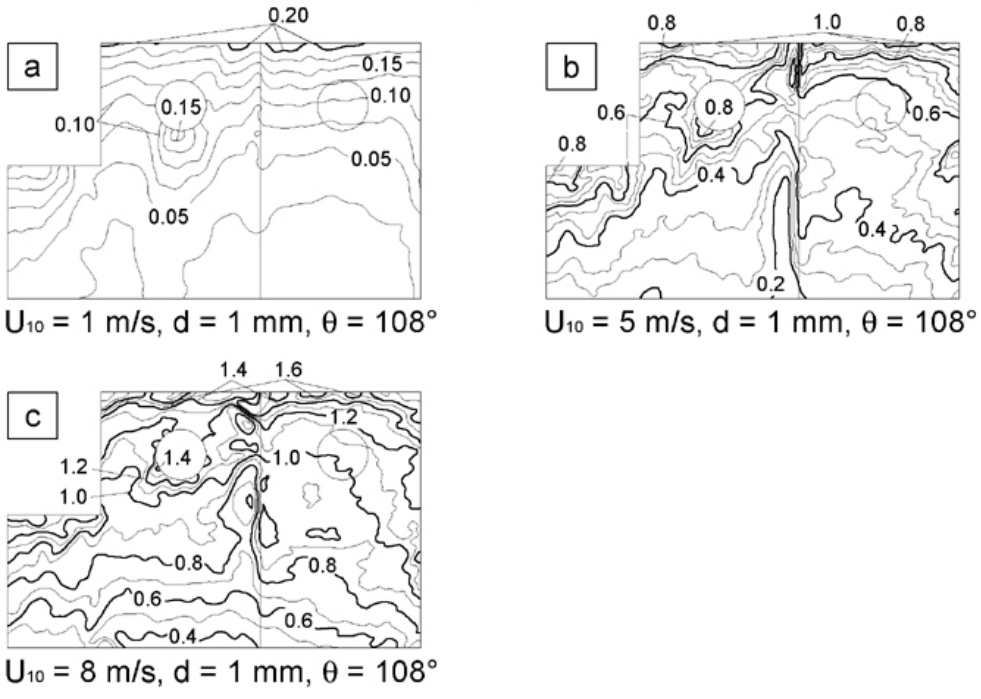

Figure 5. Contours of specific catch ratio (driving rain to horizontal rainfall ratio) at the east brick facade for wind direction θ = 108°, raindrop diameter d = 1 mm, for (a) U_{10} = 1 m/s, (b) U_{10} = 5 m/s and (c) U_{10} = 8 m/s. Bold line contour intervals are 0.2. For clarity, the circumference of the window at the right is indicated

ϕ = 225°. (Fig. 6). The specific catch ratio increases from bottom left to top right. This is in correspondence with the observations in Figure 4 where increased wind speed has been found near the vertical and top edge. For U_{10} = 5 and 8 m/s, the vertical edge receives considerably more rain than the top edge. The influence of the aperture is rather limited.

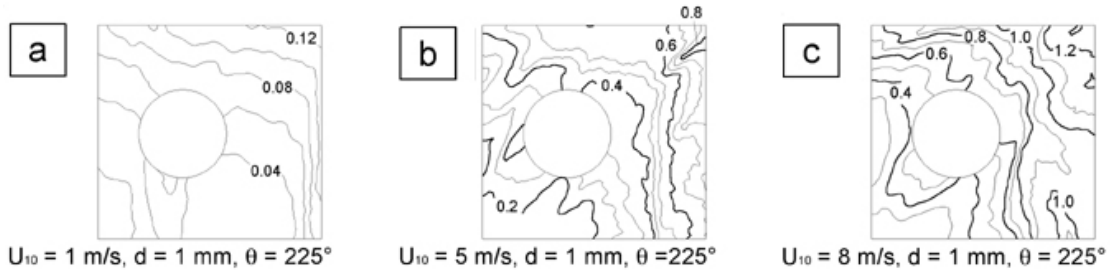

Figure 6. Contours of specific catch ratio (driving rain to horizontal rainfall ratio) at the back (west) face of the free-standing terrace wall. Wind direction θ = 225°, raindrop diameter d = 1 mm, for (a) U_{10} = 1 m/s, (b) U_{10} = 5 m/s and (c) U_{10} = 8 m/s. Bold line contour intervals are 0.2.

ϕ = 288°. (Fig. 7). The specific catch ratio increases from bottom to top as a result of the skimming flow over the roof. The effect of the skimming flow along the south facade is of less importance. The reason was indicated before: the recession of the free-standing wall compared to the south facade. The influence of the aperture is limited.

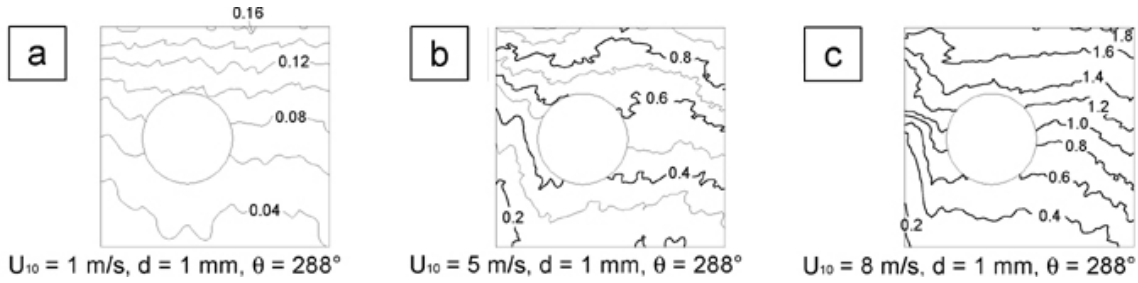

Figure 7. Contours of specific catch ratio (driving rain to horizontal rainfall ratio) at the back (west) face of the free-standing terrace wall. Wind direction θ = 288°, raindrop diameter d = 1 mm, for (a) U10 = 1 m/s, (b) U10 = 5 m/s and (c) U10 = 8 m/s. Bold line contour intervals are 0.2.

4 Discussion

The numerical study has indicated that for wind direction (108°), i.e. perpendicular to the east facade, the specific catch ratio near the aperture is on average about 40% higher than near the window with similar geometry at the right. The wetting pattern is stretched towards the bottom left, a feature that also shows in reality (Fig. 1). Nevertheless, one would expect higher specific catch ratio values around the entire circumference of the aperture, not only at the bottom left. Furthermore, another contribution to the wetting (apart from direct driving rain impact) might be considered: rain falling on the bottom half cylinder surface of the aperture. It can be absorbed by the bricks or, if these are saturated, rain water will run down the wall. It is not quite

clear to what extent this effect contributes to the overall staining. It can not be held responsible for the specific shape of the wetting pattern that is stretched towards the bottom left. This must be due to the influence of the direct driving rain impact.
The other two wind directions do not show such high values near the aperture. Isolated staining patterns or staining gradients were not observed at the facade facing the terrace. Nevertheless, specific catch ratio values here (especially near the side and top edges) can be quite high.
It is strange that staining patterns are observed at the east facade, whereas the prevalent wind direction for driving rain in these regions is south-west. The company states that the staining patterns have not changed in time since they were first noticed, three years ago during the first winter after construction. The authors think that the staining patterns have developed during one or more driving rain events with east wind direction. It is possible that parts of the facade have remained wet for a long time during winter, allowing dirt particles to be attached to these parts causing permanent stains, by the process described by Camuffo et al. (1982). A thorough investigation of all phenomena must take into account the specific wind and rain data of the site (step 4 to 6 in the model, see section 2). Unfortunately, wind and rain data at the present site are not available. Wind and rain data of a nearby weather station could be used, but as rain data can significantly differ on short distances and the stains are expected to be the result of one or more specific rain events, this option was not pursued.

5 CONCLUSIONS

A numerical method based on Computational Fluid Dynamics has been applied to study the relationship between driving rain and facade disfigurement by direct driving rain impact. The surface soiling pattern around the circular aperture could partly be explained by the use of the numerical method.
This paper is intended to be a first step in the (numerical) modelling of surface soiling of building facades by driving rain. Further research will comprise application and verification of the present model for other building configurations and the extension of the model to account for other soiling phenomena (run-off).

References

Blocken, B. & Carmeliet, J. 2000a. Driving rain on building envelopes – I, numerical estimation and full-scale experimental verification. Journal of Thermal Envelope and Building Science 24(1): 61-85.

Blocken, B. & Carmeliet, J. 2000b. Driving rain on building envelopes – II, representative experimental data for driving rain estimation. Journal of Thermal Envelope and Building Science 24(2): 89-110.

Blocken, B. & Carmeliet, J. 2002. Spatial and temporal distribution of driving rain on a low-rise building. Wind and Structures 5(5): 441-462.

Camuffo, D., Del Monte, M., Sabbioni, C. & Vittori, O. 1982. Wetting, deterioration and visual features of stone surfaces in an urban area. Atmospheric Environment 16(9): 2253-2259.

Choi, E.C.C. 1993. Simulation of wind-driven-rain around a building. Journal of Wind Engineering and Industrial Aerodynamics 46&47: 721-729.

Etyemezian, V., Davidson, C.I., Zufall, M., Dai, W., Finger, S. & Striegel, M. 2000. Impingement of raindrops on a tall building. Atmospheric Environment 34: 2399-2412.

Hangan, H. 1999. Wind-driven rain studies. A C-FD-E approach. Journal of Wind Engineering and Industrial Aerodynamics 81: 323-331.

Karagiozis, A., Hadjisophocleous, G. & Cao, S. 1997. Wind-driven rain distributions on two buildings. Journal of Wind Engineering and Industrial Aerodynamics 67&68: 559-572.

Kim, S-E., Choudhury, D. & Patel, B. 1997. Computations of complex turbulent flows using the commercial code FLUENT. Proceedings of the ICASE/LaRC/AFOSR Symposium on Modelling Complex Turbulent Flows, Hampton, Virginia.

Kim, S-E. & Choudhury, D. 1995. A near-wall treatment using wall functions sensitized to pressure gradient. Fluids Engineering Division – ASME: 217 (Separated and Complex Flows).

Lakehal, D., Mestayer, P.G., Edson, J.B., Anquetin, S. & Sini, J.-F. 1995. Eulero-Lagrangian simulation of raindrop trajectories and impacts with the urban canopy. Atmospheric Environment 29(23): 3501-3517.

Sankaran, R. and Paterson, D.A. 1995. Computation of rain falling on a tall rectangular building. Proceedings of 9ICWE, New Delhi, India.

Shih, T-H., Liou, W.W., Shabbir, A. & Zhu, J. 1995. A new k-ε eddy-viscosity model for high Reynolds number turbulent flows – model development and validation. Computers and Fluids 24(3): 227-238.

Van Mook, F.J.R. 1999. Full-scale measurements and numeric simulations of driving rain. Proceedings 10ICWE, Copenhagen, 1145-1152.

Van Mook, F.J.R., De Wit, M.H. & Wisse, J.A. 1997. Computer simulation of driving rain on building envelopes. Proceedings of 2EACWE, Genova, Italy, 1059-1066.

Wieringa, J. 1992. Updating the Davenport roughness classification. Journal of Wind Engineering and Industrial Aerodynamics 41-44: 357-368.

Wisse, J.A. 1994. Driving rain, a numerical study. Proceedings of 9th Symposium on Building Physics and Building Climatology. Dresden, September.